Eosinophils regulate intra-adipose axonal plasticity

Xia Meng[a,b,c,1], Xinmin Qian[a,b,c,1], Xiaofan Ding[a,b,c,1], Wenjing Wang[d,1], Xia Yin[d,2], Guanglei Zhuang[d,2], and Wenwen Zeng[a,b,c,2]

[a]Institute for Immunology and School of Medicine, Tsinghua University, Beijing 100084, China; [b]Tsinghua-Peking Center for Life Sciences, Tsinghua University, Beijing 100084, China; [c]Beijing Key Laboratory for Immunological Research on Chronic Diseases, Beijing 100084, China; and [d]Shanghai Key Laboratory of Gynecologic Oncology, Ren Ji Hospital, School of Medicine, Shanghai Jiao Tong University, Shanghai 200127, China

Edited by Tak Mak, Medical Biophysics and Immunology, University of Toronto, Toronto, Canada; received July 2, 2021; accepted November 23, 2021

Sympathetic innervation regulates energy balance, and the nerve density in the adipose tissues changes under various metabolic states, resulting in altered neuronal control and conferring resilience to metabolic challenges. However, the impact of the immune milieu on neuronal innervation is not known. Here, we examined the regulatory role on nerve plasticity by eosinophils and found they increased cell abundance in response to cold and produced nerve growth factor (NGF) in the white adipose tissues (WAT). Deletion of *Ngf* from eosinophils or depletion of eosinophils impairs cold-induced axonal outgrowth and beiging process. The spatial proximity between sympathetic nerves, IL-33–expressing stromal cells, and eosinophils was visualized in both human and mouse adipose tissues. At the cellular level, the sympathetic adrenergic signal induced calcium flux in the stromal cells and subsequent release of IL-33, which drove the up-regulation of IL-5 from group 2 innate lymphoid cells (ILC2s), leading to eosinophil accretion. We propose a feed-forward loop between sympathetic activity and type 2 immunity that coordinately enhances sympathetic innervation and promotes energy expenditure.

axonal plasticity | eosinophils | white adipose tissues | NGF

Sympathetic innervations mediate the efferent signals from the nervous system to the peripheral organs, including the adipose tissues, to maintain energy balance (1–4). The white adipose tissues (WAT) are the key energy storage depots and hormone-producing organs in metabolic homeostasis, dysregulation of which leads to obesity, type 2 diabetes, and other metabolic diseases (5, 6). Previous studies suggest that sympathetic arborizations are prevalent in the WAT (7, 8) and control the metabolic activities such as the cold-induced beiging process and promote the formation of the thermogenic adipocytes (7, 8), leptin production (9), and lipolysis (10). Under various physiological and pathological conditions, the sympathetic nerve density undergoes dynamic change (7, 11–14), and this process is regulated by the target adipose tissues and results in altered neuronal control (15–20). Notably, the density increases upon environmental cold exposure (11, 15) or prolonged fasting (12) and decreases under obese and diabetic conditions (7, 14, 21). The axonal plasticity represents an important layer of regulation in changing the neuronal output to the innervated organs.

The WAT harbor a diverse array of immune cells including eosinophils and group 2 innate lymphoid cells (ILC2s) (22–24). The immune subpopulations coordinate their functions in the adipose tissue metabolism, and both the cellular composition and activation state change to influence energy balance (25, 26). For instance, the roles of eosinophils have been expanded beyond parasite immunity to metabolic health, and alteration in the number of eosinophils in the WAT affects glucose homeostasis (27). The paralleled progress in revealing the crucial functions of neural innervation and immune reactions in the adipose tissues has promoted us to investigate the interrelationship between the immune factors and neuronal innervation. Particularly, it is largely unknown how the immune milieu may affect axonal plasticity and how their highly dynamic nature in response to metabolic and immunological challenges may impact the local neuronal control.

In this study, we investigated the regulatory role of axonal plasticity by immune components. We found that eosinophils expressed nerve growth factor (NGF) and promoted sympathetic axonal outgrowth. We generated *Ngf* conditional knockout allele ($Ngf^{fl/fl}$), and $Epx^{iCreERT2}$ knock-in mouse to drive eosinophil-specific genetic recombination. Deletion of *Ngf* in immune cells through crossing $Ngf^{fl/fl}$ to Vav^{iCre}, or eosinophils through crossing $Ngf^{fl/fl}$ to $Epx^{iCreERT2}$, resulted in impairments of axonal outgrowth and beiging upon cold challenge. Depletion of eosinophils through administration of anti–IL-5 neutralization antibody also led to reduced axonal outgrowth. We further showed that similar to the predominant sympathetic innervation in the mouse WAT at multiple anatomical locations such as inguinal, mesenteric, and perigonadal fats, the nerve fibers were primarily sympathetic in the human adipose tissues. The spatial proximity between the sympathetic nerves, IL-33–expressing stromal cells, and eosinophils was observed in both mouse and human fats. The stromal IL-33 signaled to ILC2s to induce IL-5 production for eosinophil accumulation. Thus, the *Il33*-deficient mice displayed defects in axonal outgrowth. Vice versa, treatment with recombinant IL-33 led to sympathetic axonal outgrowth. Lastly, we revealed that stimulation with adrenergic neurotransmitter norepinephrine (NE) or α1 adrenergic receptor agonist elicited calcium flux in the adipose stromal cells and IL-33 release. The chemogenetic sympathetic activation through administration of clozapine-*N*-oxide (CNO) into $Th^{CreERT2}$;*hM3Dq* mice or cold exposure was sufficient to induce production of IL-5. The results together suggest a feed-forward mechanism initiated by sympathetic activation and coordinated by the type 2 immune response, which promotes

Significance

Neuronal innervation in the adipose tissues plays a crucial role in regulating adipose thermogenic capacity and metabolic homeostasis. The tissue-wide nerves display a large extent of structural plasticity under physiological and pathological conditions that alter the neuronal control of metabolic states. We find here that neuronal plasticity is regulated by immune cells, which constitutes an appealing way to reshape neural-controlled energy balance by targeting immune components.

Author contributions: X.M., X.Q., and W.Z. designed research; X.M., X.Q., X.D., W.W., X.Y., and G.Z. performed research; W.W., X.Y., and G.Z. contributed new reagents/analytic tools; X.M. and X.Q. analyzed data; X.D. provided the initial preliminary observation; and X.M., X.Q., and W.Z. wrote the paper.

The authors declare no competing interest.

This article is a PNAS Direct Submission.

[1]X.M., X.Q., X.D., and W.W. contributed equally to this work.

[2]To whom correspondence may be addressed. Email: wenwenzeng@tsinghua.edu.cn, zhuangguanglei@gmail.com, or yinxia2@aliyun.com.

This article contains supporting information online at http://www.pnas.org/lookup/suppl/doi:10.1073/pnas.2112281119/-/DCSupplemental.

Published January 18, 2022.

neuronal innervation and enhances energy consumption. The findings here implicated an intervention strategy to alter the sympathetic neuronal output by modifying immune balance within the target organs for treating metabolic disorders.

Results

NGF Was Up-Regulated in Eosinophils upon Cold Exposure, which Promoted Sympathetic Axonal Outgrowth. Whole-mount immunostaining and 3D volume fluorescence imaging of tyrosine hydroxylase (TH) and CD45, labeling the sympathetic nerves and immune cells, respectively, revealed a close spatial relationship between nerves and immune cells in the inguinal WAT (iWAT) (Fig. 1*A*; Video S1). From the 3D images, 37 ± 6% (mean ± SEM) of the immune cells were detected within a distance of 30 μm and 76 ± 7% (mean ± SEM) within 60 μm from axonal arborization (Fig. 1*B*), which prompted us to investigate the potential regulation of nerve plasticity by the immune milieu. The mice housed at a thermoneutral (TN) condition (32 °C) were subjected to cold temperature exposure (cold, 4 °C), and NGF, the neurotrophic factor critical for sympathetic neurite growth, was detected in the iWAT, measured by enzyme-linked immunosorbent assay (ELISA) in the tissue homogenates (Fig. 1*C*). The immune cells were then sort purified from the enzymatically digested iWAT post–cold stimulation, and *Ngf* expression was determined by real-time quantitative PCR (qPCR). The immune subtypes showed *Ngf* expression in eosinophils identified by $CD11b^{+}Siglec\text{-}F^{+}$ gated within the $CD45^{+}$ population (Fig. 1*D*; *SI Appendix*, Fig. S1). The expression of *Ngf* was up-regulated in eosinophils in response to the cold challenge (Fig. 1*E*). Eosinophils were then isolated from the peritoneal cavity induced by intraperitoneal treatment of recombinant IL-33 and cultured in the presence of IL-5. Increased NGF release was detected in response to compound 48/80 (C48/80) stimulation measured by ELISA, which triggers eosinophil degranulation (Fig. 1*F*). The previous study showed that a significant increase of eosinophil numbers occurs in the WAT in response to the cold stimulation (28). We observed that the proportion of eosinophils in the $CD45^{+}Ter119^{-}$ immune cells increased upon transfer of mice from thermoneutral condition to a cold environment, assessed by flow cytometry (Fig. 1 *G* and *H*).

Whole-mount immunostaining showed that the eosinophils and the sympathetic nerves, stained with antibodies against Siglec-F and TH, respectively, displayed spatial proximity in the iWAT (Fig. 1*I*; Video S2). From the images, 41 ± 5% (mean ± SEM) of the eosinophils resided within a distance of 30 μm and 75 ± 5% (mean ± SEM) within 60 μm from nerves (Fig. 1*J*). The eosinophil density increased significantly upon cold exposure (Fig. 1*K*). Furthermore, we isolated the eosinophils from peritoneal cavity of mice intraperitoneally injected with recombinant IL-33. The eosinophils promoted axonal outgrowth when cocultured with sympathetic neurons from the superior cervical ganglia (SCG), which was inhibited by anti-NGF neutralization antibody, examined by immunohistochemical analysis against TH (Fig. 1*L*). Both the axonal branching and growth were enhanced, quantified by the number of intersections plotted against the distance from the ganglia body, and the extrapolated area under the curve (AUC) (Fig. 1*M*) was analyzed by NeuriteJ (29). Together, the data provided evidence that eosinophils promoted sympathetic axonal outgrowth.

Eosinophils Regulated the Intra-Adipose Axonal Plasticity and the Beiging Process. To provide genetic evidence for the cell-specific role of NGF in regulating intra-adipose axonal plasticity, we generated an *Ngf* conditional knockout mouse line $NGF^{fl/fl}$ with the CRISPR/Cas9 strategy (*SI Appendix*, Fig. S2*A*). *Ngf* was deleted in the hematopoietic cells by crossing $NGF^{fl/fl}$ to Vav^{iCre}, and the genetic recombination was confirmed in the lymph node by qPCR (*SI Appendix*, Fig. S2*B*); no deletion was observed in the salivary gland, which highly expresses *Ngf* (*SI Appendix*, Fig. S2*C*) (30). Whole-mount immunostaining using antibodies against TH and Stathmin 2 (STMN2) was carried out to label sympathetic nerves and regenerating axons, respectively. The cold-elicited sympathetic outgrowth was impaired in the iWAT from the $Vav^{iCre};NGF^{fl/fl}$ mice when compared with the control mice, showing the decreased density of sympathetic nerves and reduced STMN2 signal in response to cold challenge (Fig. 2 *A* and *D*). We then examined the expression of the genes associated with the beiging process accordingly, including *Ucp1*, *Dio2*, *Cidea*, and *Pgc1a* (31). Decreased induction of beiging-associated genes was detected by qPCR (Fig. 2*E*), and fewer multilocular beige cells were observed on hematoxylin and eosin (HE) staining of the iWAT from $Vav^{iCre};NGF^{fl/fl}$ mice compared to control animals upon cold exposure (Fig. 2 *F* and *G*).

To examine the contribution of NGF expressed in nonimmune cells such as $CD31^{+}$ endothelial cells, stromal cells, and adipocytes to the acutely enhanced thermogenic capacity (*SI Appendix*, Fig. S2*D*), we transplanted bone marrow cells from wild-type (WT) mice into the recipient $NGF^{fl/fl}$ or $Vav^{iCre};NGF^{fl/fl}$ mice that had been lethally irradiated. We then examined the beiging process of the mice housed at the TN condition or exposed to cold for 6 d. The $NGF^{fl/fl}$ and $Vav^{iCre};NGF^{fl/fl}$ recipients reconstituted with WT hematopoietic cells showed comparable up-regulation of *Ucp1*, *Dio2*, *Cidea*, and *Pgc1a*, supporting the important role of immune cell–derived NGF for sympathetic outgrowth and beiging (*SI Appendix*, Fig. S2*E*). Also, Vav^{iCre} is known to express Cre in endothelial cells, and to determine whether endothelial NGF could function as a prosurvival factor for angiogenesis in an autocrine manner (32, 33), we examined the vascularization in those animals. $Vav^{iCre};NGF^{fl/fl}$ mice displayed comparable vascularization with the control $NGF^{fl/fl}$ mice, suggesting that endothelial NGF was dispensable for WAT vascularization (*SI Appendix*, Fig. S2 *F* and *G*).

To further determine the role of NGF derived from eosinophils in regulating intra-adipose axonal plasticity, we generated an $Epx^{iCreERT2}$ mouse line by inserting an *iCre-ERT2* cassette following the endogenous eosinophil peroxidase (*Epx*) gene separated by a P2A polyprotein cleavage site with the CRISPR/Cas9 strategy (*SI Appendix*, Fig. S2*H*). $Epx^{iCreERT2}$-mediated gene recombination in eosinophils was confirmed by crossing $Epx^{iCreERT2}$ to *Ai32* reporter mouse harboring flox-stop-flox *ChR2-EYFP* cassette, which showed EYFP expression in eosinophils ($CD11b^{+}SiglecF^{+}$) but not in other immune subtypes post–tamoxifen induction (*SI Appendix*, Fig. S2*I*). *Ngf* was then deleted in eosinophils by crossing $Ngf^{fl/fl}$ to $Epx^{iCreERT2}$. Whole-mount staining revealed that the cold-elicited sympathetic outgrowth was impaired in the iWAT from the $Epx^{iCreERT2};Ngf^{fl/fl}$ mice when compared with the control $Epx^{iCreERT2}$ mice, showing reduced density of sympathetic nerves and STMN2 signal post–cold exposure (Fig. 3 *A* and *D*). Meanwhile, reduced levels of UCP1 assayed by immunostaining and fewer multilocular beige cells on HE in iWAT from $Epx^{iCreERT};Ngf^{fl/fl}$ mice compared to control animals were observed upon cold exposure (Fig. 3 *E*–*H*). Collectively, the results indicated that NGF derived from the eosinophils regulated the intra-adipose axonal plasticity, which influenced the cold-induced beiging process.

The Intra-Adipose Axonal Plasticity Is Regulated by IL-5 Signal. To investigate the role of eosinophils in regulating axonal plasticity in vivo, we delivered the anti–IL-5 neutralization antibody through intraperitoneal administration. The depletion of eosinophils in the iWAT was detected by flow cytometric analysis, showing that the proportion of eosinophils in the immune cells was drastically decreased after anti–IL-5 antibody treatment (Fig. 4 *A* and *B*). Whole-mount staining showed that the cold-elicited axonal outgrowth was decreased when the eosinophils

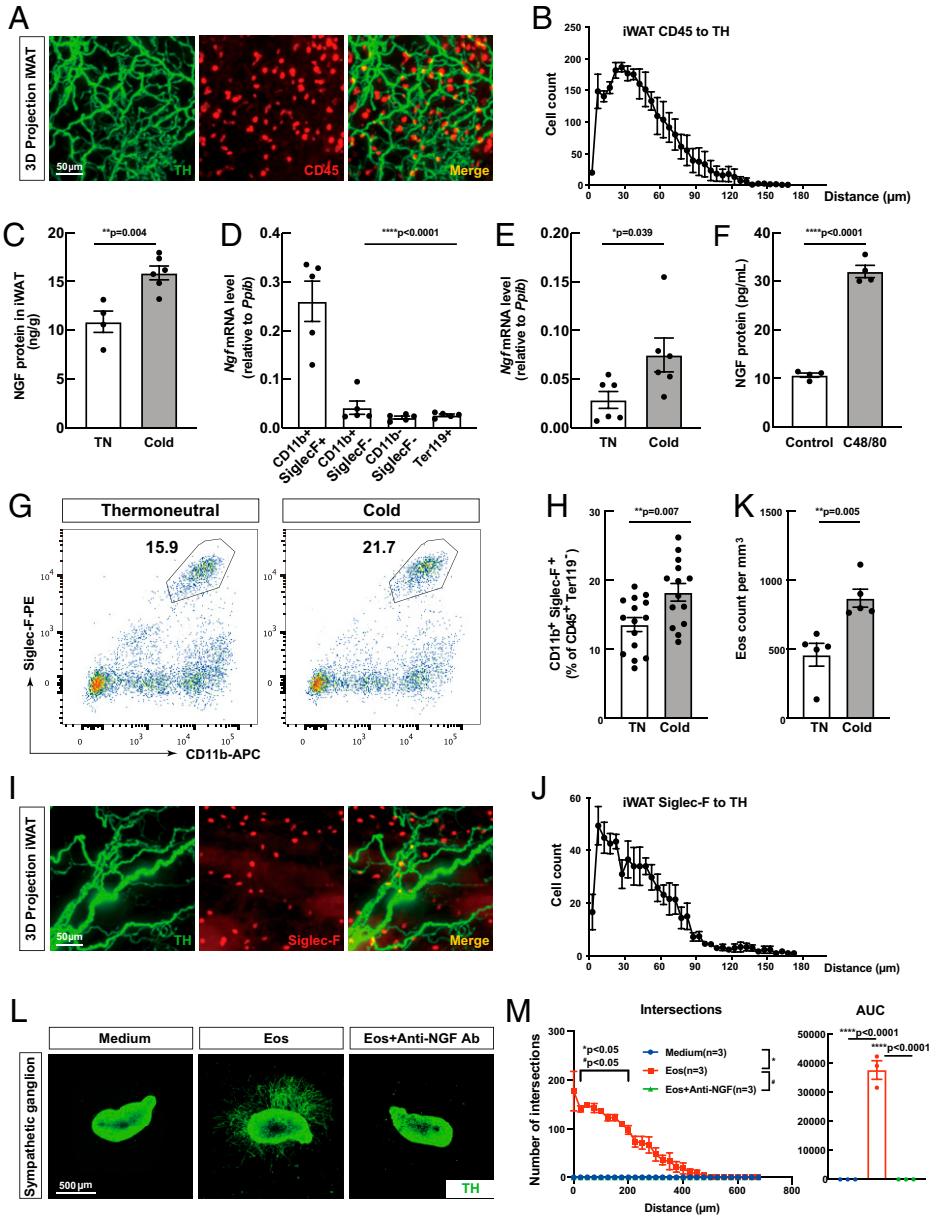

Fig. 1. Eosinophils express NGF and promotes sympathetic axonal outgrowth. (*A* and *B*) The iWAT were processed for the whole-mount immunostaining and volume fluorescence imaging at 12.6× magnification on the lightsheet microscope. The 3D-projection images of costaining of TH and CD45 were shown with a depth of 500 μm (*A*). The distances from $CD45^+$ immune cells to TH^+ nerves were plotted (*B*). $n = 3$ mice. (*C*) The mice housed at TN condition ($n = 4$) or subjected to cold challenge (cold) for 2 d ($n = 6$). The iWAT were homogenized and ELISA was performed to determine the levels of NGF. (*D*) The immune subsets were sort purified from the iWAT of cold-challenged WT mice and analyzed for the expression of *Ngf* by qPCR. $n = 5$ mice. (*E*) Eosinophils ($CD11b^+Siglec\text{-}F^+$) were sort purified from the iWAT of mice housed at the TN condition or cold challenged, and the expression of *Ngf* was analyzed by qPCR. $n = 6$ mice for each group. (*F*) Eosinophils ($Siglec\text{-}F^+CCR3^+$) were sort purified from the peritoneal cavity of mice post–IL-33 induction, and the release of NGF was detected by ELISA. $n = 4$ wells for each group. (*G* and *H*) The WT mice housed at the thermoneutral condition ($n = 15$) or subjected to cold challenge ($n = 14$). Frequencies of eosinophils ($CD11b^+Siglec\text{-}F^+$) were assessed by flow cytometric analysis (*G*) and quantified (*H*). Cells were gated on $CD45^+Ter119^-$ cells. (*I*–*K*) The iWAT from the cold-challenged mice were processed for the whole-mount immunostaining and volume fluorescence imaging at 12.6× magnification on the lightsheet microscope. The 3D-projection images of costaining of TH and Siglec-F were shown with a depth of 500 μm (*I*). The distances from $Siglec\text{-}F^+$ eosinophils to TH^+ nerves were plotted ($n = 5$ mice) (*J*). The eosinophil (eos) count was presented ($n = 5$ mice for each group) (*K*). (*L* and *M*) Eosinophils were isolated from the peritoneal cavity of IL-33–induced mice and cocultured with dissected SCG in the presence of anti-NGF neutralization antibody (Ab) in vitro. The sympathetic neurons were examined by immunostaining of anti-TH (*L*). NeuriteJ was used to quantify the axonal outgrowth. The number of intersections indicating the neurite branching was plotted against the distance from the ganglia body, and the AUC was extrapolated as an indicator of axonal growth (*M*). $n = 3$ SCG for each group. Data are presented as mean ± SEM. *P* values were calculated by two-tailed unpaired *t* test (*C*, *E*, *F*, *H*, *K*), ordinary one-way ANOVA with Dunnett's multiple comparisons test (*D*), two-way ANOVA of repeated measures and Bonferroni's post hoc test (*M*, *Left*), and ordinary one-way ANOVA with Tukey's multiple comparisons test (*M*, *Right*). ns (nonsignificant) $P > 0.05$, $*P \le 0.05$, $**P \le 0.01$, $***P \le 0.001$, $****P \le 0.0001$. APC, allophycocyanin.

were depleted, evidenced by an impaired increase of the TH-stained sympathetic nerves in the anti–IL-5 antibody-treated mice in response to cold stimulation (Fig. 4 *C* and *D*). Consistently, STMN2 was reduced, demonstrating impaired axonal outgrowth (Fig. 4 *E* and *F*). Cold challenge increased the messenger RNA (mRNA) levels of the beiging-associated genes; however, the induction was significantly impaired upon depletion of eosinophils (Fig. 4*G*). In parallel, fewer

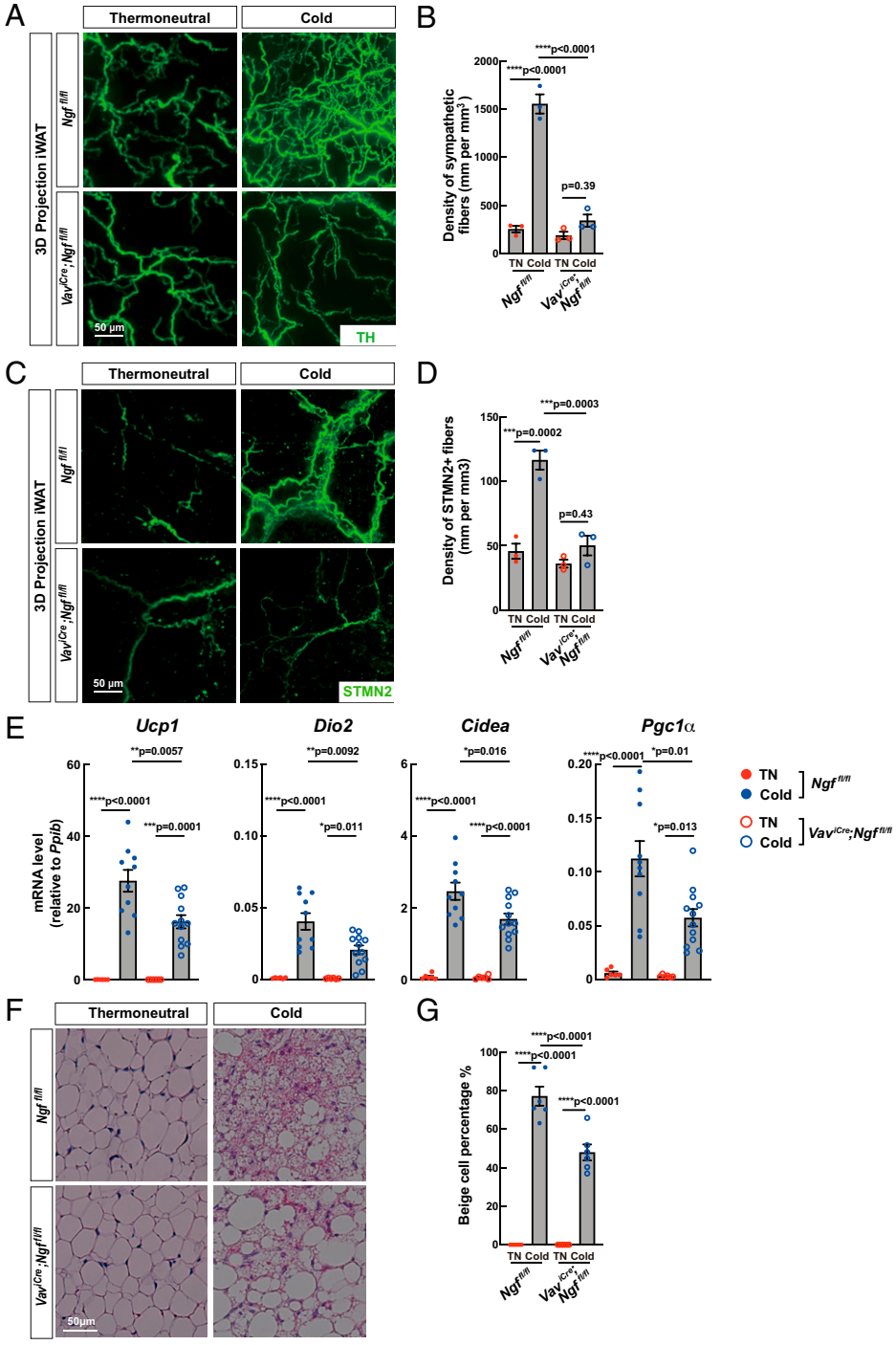

Fig. 2. NGF derived from immune cells regulates intra-adipose axonal outgrowth and beiging process induced by cold exposure. (*A–D*) The mice with indicated genotypes housed at the TN condition were subjected to cold challenge for 6 d. The iWAT were processed for the whole-mount immunostaining and volume fluorescence imaging at 12.6× magnification on the lightsheet microscope. The 3D-projection images of TH (*A*) and STMN2 (*C*) stained with the respective antibodies were shown from a depth of 500 μm. The density for TH^+ or $STMN2^+$ nerve fiber length was quantified (*B* and *D*). $n = 3$ mice for each group. (*E*) Expression levels of the beiging-related genes in iWAT from mice housed at the TN condition or cold challenged for 6 d were determined by the qPCR analysis. $n = 6$ for $Ngf^{fl/fl}$ TN, $n = 10$ for $Ngf^{fl/fl}$ cold, $n = 6$ for Vav^{iCre};$Ngf^{fl/fl}$ TN, and $n = 12$ for Vav^{iCre};$Ngf^{fl/fl}$ cold. (*F* and *G*) Appearance of multilocular beige cells in iWAT examined by HE staining (*F*) and the percentage of beige cells quantified (*G*). $n = 6$ lobules for each group. Data are presented as mean ± SEM. *P* values were calculated by two-way ANOVA and Tukey's post hoc test (*B*, *D*, *E*, *G*). ns $P > 0.05$, $*P \le 0.05$, $**P \le 0.01$, $***P \le 0.001$, $****P \le 0.0001$.

multilocular beige cells were detected by HE staining post–cold exposure when the eosinophils were depleted (Fig. 4 *H* and *I*). These results have together suggested that IL-5 maintained eosinophils in WAT, which were critical in mediating the intra-adipose sympathetic axonal plasticity.

Sympathetic Innervation, IL-33, and Eosinophil Distribution in Human and Mouse Adipose Tissues. IL-33 is one key cytokine produced by stromal cells regulating the immune microenvironment and metabolic homeostasis in the WAT (22, 24, 34–41), and the deletion of *Il33* led to severely decreased eosinophils

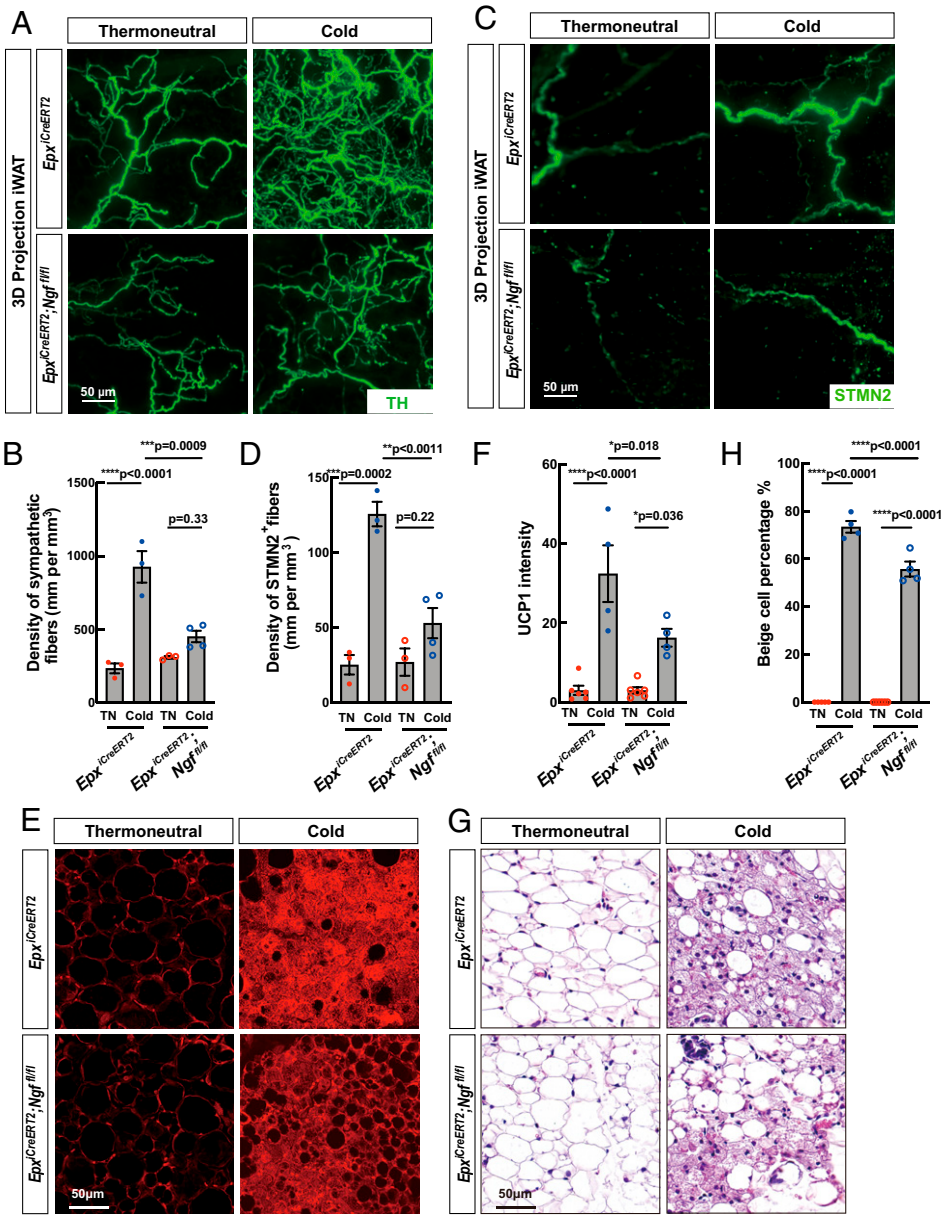

Fig. 3. NGF derived from eosinophils regulates intra-adipose axonal outgrowth and beiging process induced by cold exposure. (*A*–*D*) The mice with the indicated genotypes housed at the TN condition were subjected to cold challenge for 3 d. The iWAT were processed for the whole-mount immunostaining and volume fluorescence imaging at 12.6× magnification on the lightsheet microscope. The 3D-projection images of TH (*A*) and STMN2 (*C*) stained with the respective antibodies were shown from a depth of 500 μm. The nerve fiber length was quantified for TH and STMN2 (*B* and *D*). $n = 4$ for $Epx^{iCreERT2}$;$Ngf^{fl/fl}$ group and $n = 3$ for the rest. (*E* and *F*) Expression of UCP1 in iWAT from mice housed at the TN condition or cold challenged for 3 d were determined by immunostaining (*E*). The UCP1 intensity was quantified by ImageJ (*F*). $n = 6$ mice for TN and $n = 4$ mice for cold. (*G* and *H*) Appearance of multilocular beige cells in iWAT examined by HE staining (*G*). The percentage of beige cells among adipocytes was quantified (*H*). $n = 5$ mice for TN $Epx^{iCreERT2}$, $n = 6$ mice for TN $Epx^{iCreERT2}$;$Ngf^{fl/fl}$ and $n = 4$ mice for cold. Data are presented as mean ± SEM. *P* values were calculated by two-way ANOVA and Tukey's post hoc test (*B*, *D*, *F*, *H*). ns $P > 0.05$, *$P \leq 0.05$, **$P \leq 0.01$, ***$P \leq 0.001$, ****$P \leq 0.0001$.

assayed in visceral WAT (40). We then determined whether the IL-33 signal affects axonal plasticity. To provide evidence for the potential interaction between nerves, immune cells, and IL-33 signal, we firstly visualized their distribution in the human and mouse fats. Adipose tissues at various anatomical locations (epiploic appendixes, omental, pelvic, abdominal wall, pelvic wall, and subcutaneous) were obtained from normal tissues of ovarian cancer patients and processed by whole-mount immunostaining and 3D volume fluorescence imaging. Sympathetic nerves were shown to be the predominant nerve subtype stained by TH (*SI Appendix*, Fig. S3*A*) and colabeled by TH and the pan-neuronal marker β-tubulin III (Tuj1) (*SI Appendix*, Fig. S3*B* and Video S3). Very few signals costaining Tuj1 and vesicular acetylcholine transporter (VAChT) were detected, the latter of which labeled the parasympathetic nerves, though some VAChT-positive non-neuronal cells were observed (*SI Appendix*, Fig. S4*A*). Costaining of TH and IL-33 in mouse iWAT was performed, which showed that IL-33 signal was near sympathetic nerves on whole-mount staining, with 58 ± 6% (mean ± SEM) of the IL-33–expressing cells distributed within a distance of 30 μm and 85 ± 4% (mean ± SEM) within 60 μm (Fig. 5 *A* and *B*; Video S4). In human adipose tissues, the clusters of IL-33–expressing stromal cells, eosinophils or total immune cells, and sympathetic nerves were detected by

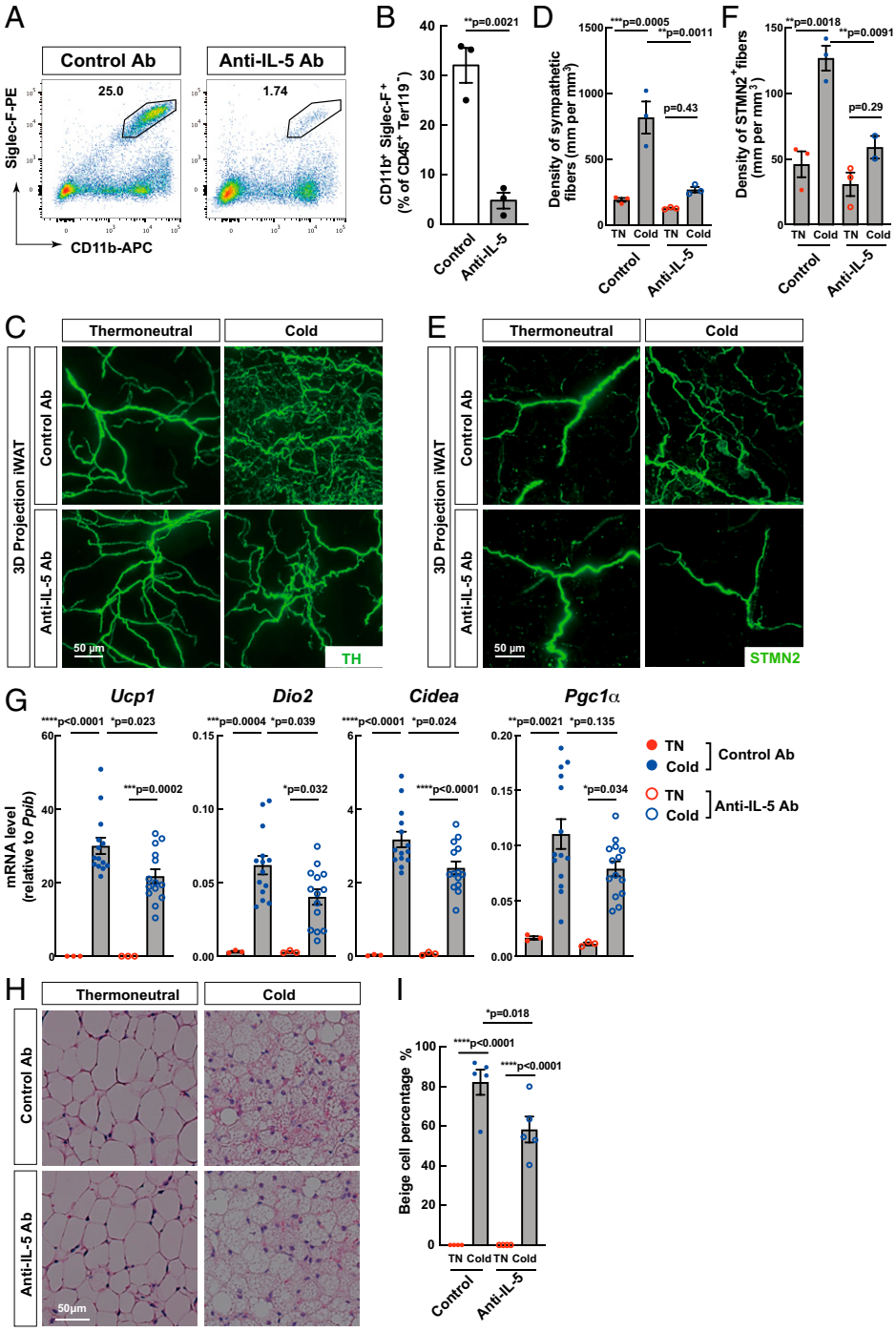

Fig. 4. IL-5 signal regulates eosinophils and intra-adipose axonal outgrowth. (*A* and *B*) The WT mice housed at the TN condition were subjected to cold challenge for 4 d. The mice received the intraperitoneal injection of anti–IL-5 antibody or control IgG antibody twice, 3 d prior to cold challenge and 1 d at cold treatment. The abundance of eosinophils was analyzed by flow cytometry post–antibody treatment (*A*). Cells were gated on $CD45^+Ter119^-$ cells. The percent of eosinophils ($CD11b^+Siglec\text{-}F^+$) in $CD45^+Ter119^-$ cells was quantified (*B*). $n = 3$ mice. (*C*–*F*) The iWAT from the antibody-treated mice were processed for the whole-mount immunostaining and 3D volume fluorescence imaging at 12.6× magnification on the lightsheet microscope. The 3D-projection images of TH (*C*) and STMN2 (*E*) stained with the respective antibodies were shown from a depth of 500 μm. The nerve fiber length was quantified (*D* and *F*). $n = 2$ mice for STMN2 anti-IL5 cold, $n = 3$ for the rest. (*G*) Expression levels of the beiging-related genes in iWAT were determined by the qPCR analysis. $n = 3$ for TN and $n = 14$ for the cold challenge. (*H* and *I*) Appearance of multilocular beige cells in iWAT was examined by HE staining, and the percentage of beige cells was quantified. $n = 4$ lobules for TN and $n = 5$ for cold. Data are presented as mean ± SEM. *P* values were calculated by two-tailed unpaired *t* test (*B*) and two-way ANOVA and Tukey's post hoc test (*D*, *F*, *G*, *I*). ns $P > 0.05$, $*P \le 0.05$, $**P \le 0.01$, $***P \le 0.001$, $****P \le 0.0001$. Ab, antibody; APC, allophycocyanin.

costaining of IL-33, Siglec-8, or CD45 with Tuj1 (Fig. 5*C*). Collectively, the data indicated that the crosstalk between the nerves and eosinophils was present in both mice and human adipose tissues.

IL-33 Regulates the Intra-Adipose Axonal Plasticity. We then assessed the effect of loss of IL-33 on axonal plasticity in WAT. Flow cytometric analysis of iWAT from "Red5" IL-5-tdTomato reporter mice (42) showed that IL-5 was mainly derived from

ILC2s (Fig. 6 *A* and *B*). The ILC2s isolated from the iWAT were predominantly ST2$^+$, which confer responsiveness to IL-33 (Fig. 6*C*) and produced IL-5 when stimulated with IL-33 in vitro (Fig. 6*D*). Interestingly, the ST2$^+$, but not the ST2$^-$, subtype increased in abundance post–cold exposure (Fig. 6*E*), suggesting that the ST2 receptor was engaged via IL-33 signal. The *Il33*-deficient mouse line (*Il33*$^{-/-}$) was therefore generated with CRISPR/Cas9 strategy and genetic deletion was verified by qPCR (*SI Appendix*, Fig. S5 *A* and *B*). The WT and *Il33*$^{-/-}$ mice housed at the TN condition were subjected to cold exposure. *Il33*$^{-/-}$ displayed decreased eosinophil numbers, shown by whole-mount staining and quantification (Fig. 6 *F* and *G*). Reduced NGF was observed in the iWAT, assayed by ELISA (Fig. 6*H*). Further, impaired sympathetic outgrowth was detected when *Il33* was deleted, evidenced by reduced sympathetic density on TH staining and decreased STMN2 signal upon cold challenge (Fig. 6 *I*–*L*). Consistently, cold-induced beiging was impaired, showing reduced expression of beiging-associated genes and fewer multilocular beige cells on HE staining (*SI Appendix*, Fig. S5 *C*–*E*). Together, these data suggested that the IL-33 signal regulated axonal plasticity in the WAT.

To further verify the role of IL-33 on axonal plasticity, we administrated recombinant IL-33 into mice through intraperitoneal injection. Post–IL-33 treatment of WT mice housed at the TN condition, flow cytometric analysis showed that the eosinophils increased significantly in the iWAT, showing the increased proportion of CD45$^+$Ter119$^-$ cells in live cells and CD11b$^+$Siglec-F$^+$ cells in CD45$^+$Ter119$^-$ population, respectively (*SI Appendix*, Fig. S5 *F* and *G*). Whole-mount staining revealed that eosinophil numbers increased in the iWAT, stained by anti–Siglec-F antibody (*SI Appendix*, Fig. S5 *H* and *I*). In parallel, NGF was increased in the iWAT measured by ELISA (*SI Appendix*, Fig. S5*J*). Whole-mount staining revealed the increased sympathetic density labeled by TH and elevated axonal outgrowth by STMN2 (*SI Appendix*, Fig. S5 *K* and *L*), demonstrating that IL-33 administration promoted the axonal outgrowth.

Sympathetic Activity Drives the IL-33 to IL-5 Signal Cascade. We next investigated how the signal cascade leading to eosinophil accrual was triggered upon cold exposure. The spatial proximity between nerves and IL-33 prompted us to probe the possibility of direct crosstalk. Analysis of the single-cell transcriptome of adipose stromal cells (43) showed that among the adrenergic receptor family, adrenergic receptor α1b (*Adrα1b*) was the only member displaying prominent expression, which was highly correlated with the expression of *Il33* (Fig. 7*A*). Adrα1b belongs to the G protein–coupled receptor (GPCR) superfamily, which mediates its action by association with G proteins that activate a phosphatidylinositol-calcium second messenger system (44). We then isolated and cultured the adipose stromal cells and incubated the cells with Rhod-2 calcium indicator followed by stimulation with calcium ionophore ionomycin, NE, or the Adrα1b agonist phenylephrine (PE). Time-lapse imaging showed that increased intracellular Ca^{2+} was elicited upon stimulation by the compounds (Fig. 7 *B* and *C*; Videos S5–S8), indicating a direct cellular response evoked by the adrenergic signal. The previous study showed that an increase in Ca^{2+} concentration induces IL-33 release from normal human bronchial epithelial cells (45). In the adipose stromal cells, we also detected reduced IL-33 in the nuclei post–calcium flux analyzed by immunostaining (Fig. 7*D*). Meanwhile, the collected supernatant promoted IL-5 production by ILC2s in culture, which was impaired in ILC2s

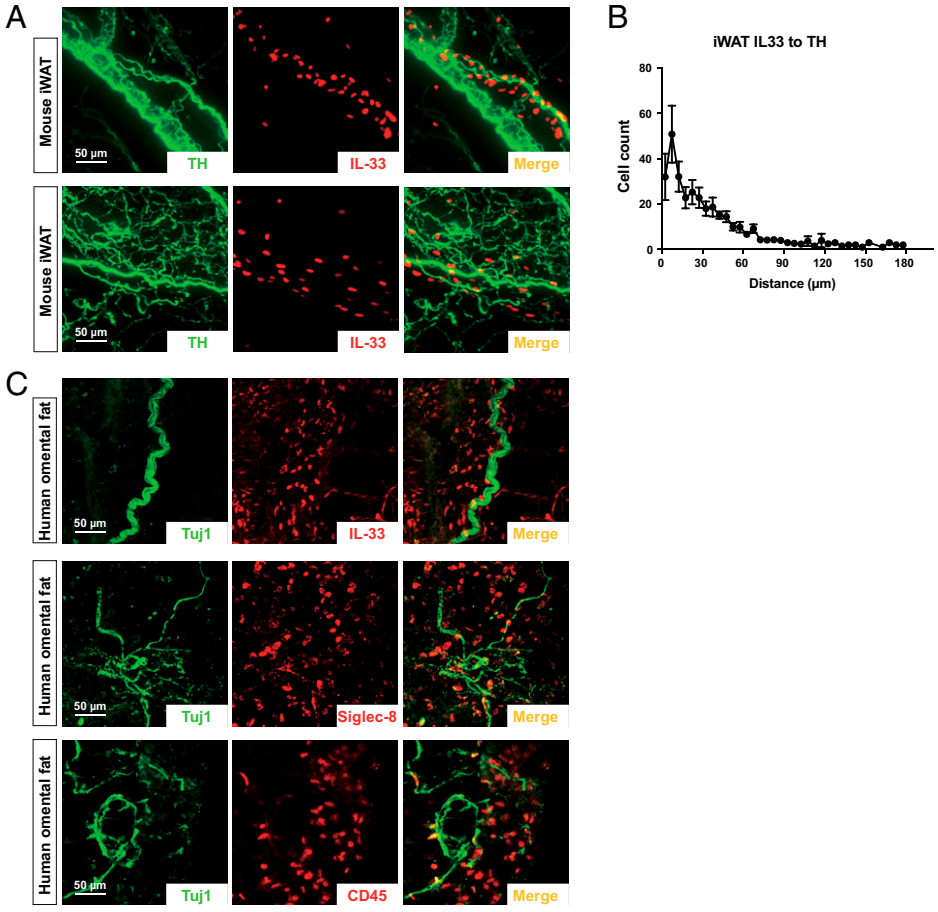

Fig. 5. The sympathetic nerves are in proximity with IL-33 and eosinophils in mouse and human adipose tissues. (*A* and *B*) The mouse iWAT were processed for the whole-mount immunostaining and volume fluorescence imaging. The 3D-projection images of TH and IL-33 adjacent to blood vessel (*A*, *Top*) and in the parenchyma (*A*, *Bottom*) were shown with a depth of 500 μm. The distance of IL-33 from nerve was plotted (*B*). $n = 7$ mice. (*C*) Human omental adipose tissues were processed by cryosections and immunostaining. The costained images of Tuj1 and IL-33, Tuj1 and Siglec-8, or Tuj1 and CD45 were shown.

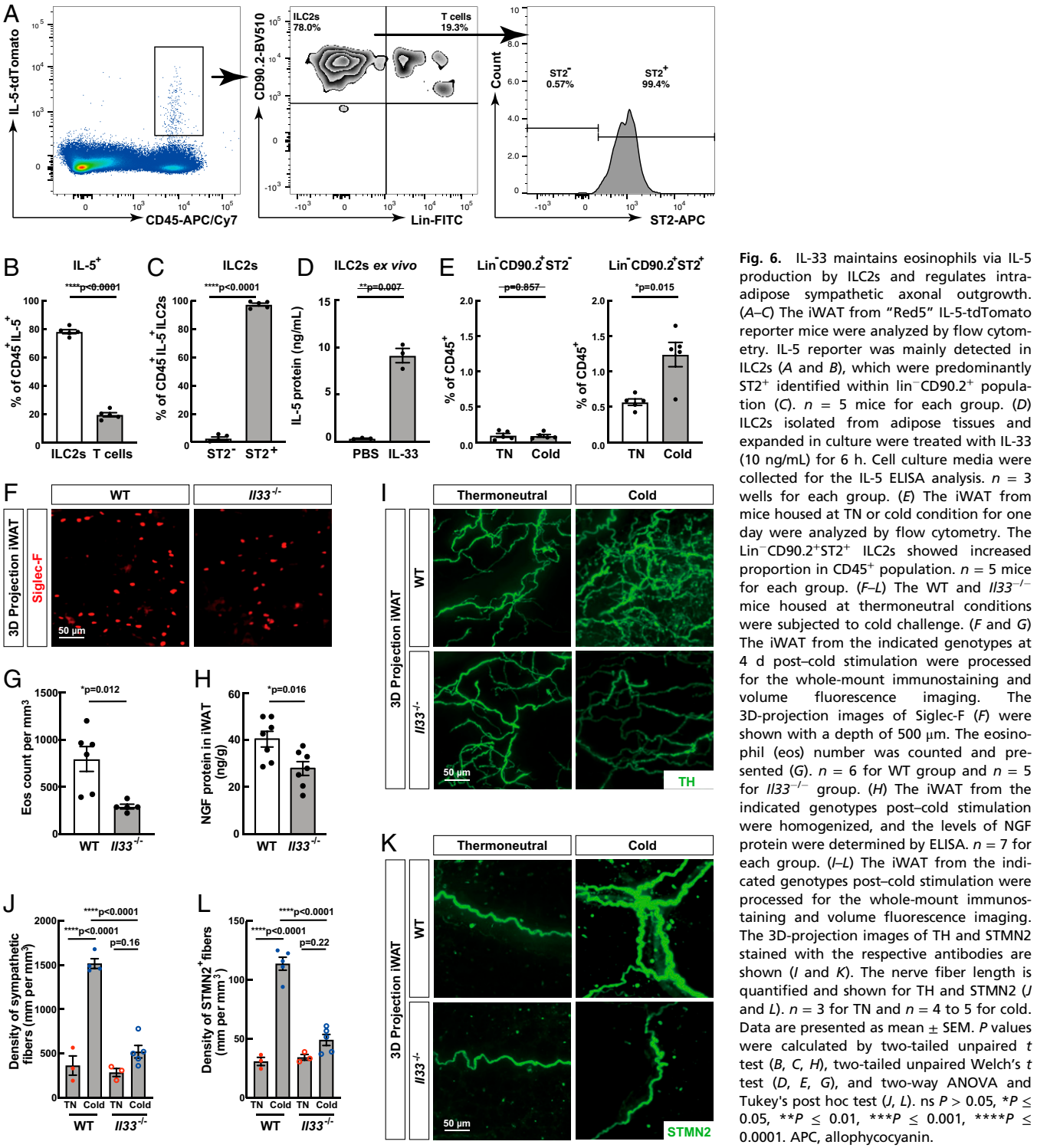

Fig. 6. IL-33 maintains eosinophils via IL-5 production by ILC2s and regulates intra-adipose sympathetic axonal outgrowth. (*A–C*) The iWAT from "Red5" IL-5-tdTomato reporter mice were analyzed by flow cytometry. IL-5 reporter was mainly detected in ILC2s (*A* and *B*), which were predominantly ST2$^+$ identified within lin$^-$CD90.2$^+$ population (*C*). n = 5 mice for each group. (*D*) ILC2s isolated from adipose tissues and expanded in culture were treated with IL-33 (10 ng/mL) for 6 h. Cell culture media were collected for the IL-5 ELISA analysis. n = 3 wells for each group. (*E*) The iWAT from mice housed at TN or cold condition for one day were analyzed by flow cytometry. The Lin$^-$CD90.2$^+$ST2$^+$ ILC2s showed increased proportion in CD45$^+$ population. n = 5 mice for each group. (*F–L*) The WT and *Il33*$^{-/-}$ mice housed at thermoneutral conditions were subjected to cold challenge. (*F* and *G*) The iWAT from the indicated genotypes at 4 d post–cold stimulation were processed for the whole-mount immunostaining and volume fluorescence imaging. The 3D-projection images of Siglec-F (*F*) were shown with a depth of 500 μm. The eosinophil (eos) number was counted and presented (*G*). n = 6 for WT group and n = 5 for *Il33*$^{-/-}$ group. (*H*) The iWAT from the indicated genotypes post–cold stimulation were homogenized, and the levels of NGF protein were determined by ELISA. n = 7 for each group. (*I–L*) The iWAT from the indicated genotypes post–cold stimulation were processed for the whole-mount immunostaining and volume fluorescence imaging. The 3D-projection images of TH and STMN2 stained with the respective antibodies are shown (*I* and *K*). The nerve fiber length is quantified and shown for TH and STMN2 (*J* and *L*). n = 3 for TN and n = 4 to 5 for cold. Data are presented as mean ± SEM. P values were calculated by two-tailed unpaired t test (*B*, *C*, *H*), two-tailed unpaired Welch's t test (*D*, *E*, *G*), and two-way ANOVA and Tukey's post hoc test (*J*, *L*). ns $P > 0.05$, $^*P \leq 0.05$, $^{**}P \leq 0.01$, $^{***}P \leq 0.001$, $^{****}P \leq 0.0001$. APC, allophycocyanin.

obtained from mice lacking a functional IL-33 receptor (*Il1rl1*$^{-/-}$) (Fig. 7 *E* and *F*) generated with CRISPR/Cas9 strategy and verified by qPCR (*SI Appendix*, Fig. S6).

The engineered GPCR hM3Dq can activate neurons in response to CNO (46). We then set out to determine whether the sympathetic activation is sufficient to drive the signal cascade using the *Th*^{CreERT2}*;hM3Dq* mice, which expressed *hM3Dq* in sympathetic neurons post–tamoxifen treatment. Upon intraperitoneal administration of CNO into *Th*^{CreERT2}*;hM3Dq* mice, we found that *Il5* expression in the iWAT and the serum IL-5 were both induced (Fig. 7 *G* and *H*). Consistently, increased serum IL-5 was detected by ELISA upon cold exposure (Fig. 7*I*). These results together suggested that activation of sympathetic neurons triggered the signal events from IL-33 release to IL-5 induction, and the sympathetic activity engaged the cellular crosstalk in a feed-forward manner to regulate the axonal plasticity.

Discussion

In this study, we sought to understand the mechanisms underlying the intra-adipose axonal plasticity. Our results collectively

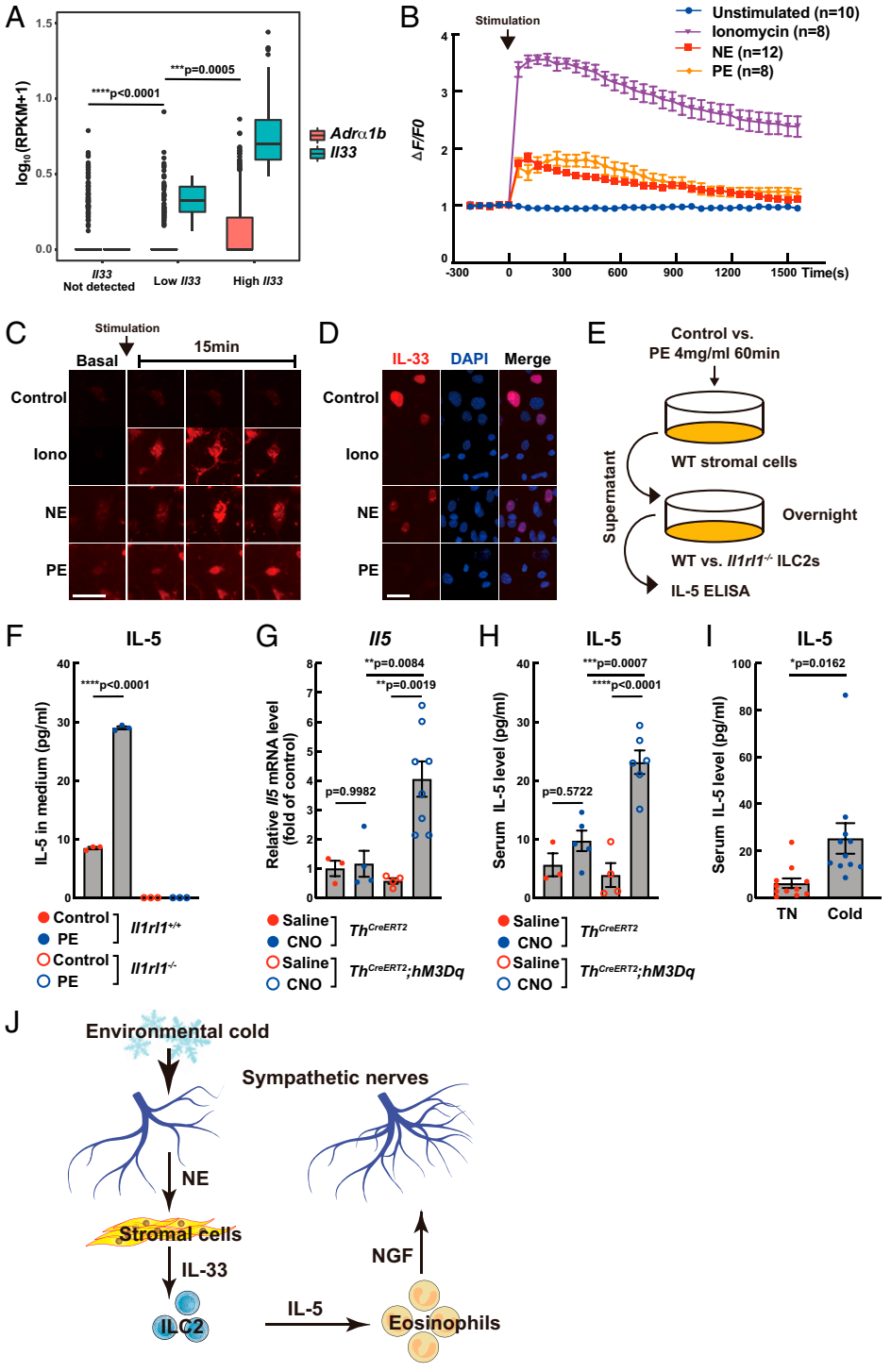

Fig. 7. Sympathetic activation promotes IL-33–IL-5 axis. (*A*) The single-cell transcriptome of iWAT (43) was analyzed, and the correlative expression of *Adrα1b* and *Il33* is shown. RPKM, reads per kilo base per million mapped reads. (*B* and *C*) The adipose stromal cells were isolated from iWAT and cultured in vitro. The cells were preloaded with Rhod-2 before being stimulated with ionomycin (Iono), NE, or PE. The time-lapse imaging (*B*) and snapshots at basal line and 15 mins after stimulation (*C*) are shown. N represents cell number, and the cells were from three mice. (*D*) The adipose stromal cells untreated or stimulated with Iono, NE, or PE were stained with IL-33. (*E* and *F*) The adipose stromal cells cultured in vitro were stimulated with PE. The conditioned medium treated with PE for 60 min was incubated with ILC2s for overnight, and IL-5 production was measured by ELISA. n = 3 wells for each group. (*G*) The mice with indicated genotypes were injected intraperitoneally with vehicle (saline) or CNO (1 mg/kg) for 6 h before iWAT were collected for qPCR. n = 3 for $Th^{creERT2}$ saline group, n = 4 for $Th^{creERT2}$ CNO group, n = 4 for $Th^{creERT2}$;*hM3Dq* saline group, and n = 8 for $Th^{creERT2}$;*hM3Dq* CNO group. (*H*) The mice with indicated genotypes were injected intraperitoneally with vehicle or CNO for 6 h before serum were collected for ELISA. n = 3 for $Th^{creERT2}$ saline group, n = 5 for $Th^{creERT2}$ CNO group, n = 4 for $Th^{creERT2}$;*hM3Dq* saline group, and n = 6 for $Th^{creERT2}$;*hM3Dq* CNO group. (*I*) The WT mice housed at the TN condition were exposed to cold for 6 h before serum were collected for ELISA analysis of IL-5. n = 11 for TN group and n = 11 for cold-treated group. (*J*) The model illustrating the feed-forward mechanism by sympathetic activation and axonal outgrowth. Sympathetic activity engages the adrenergic signaling on adipose stromal cells, which release IL-33 to enhance the production of IL-5. IL-5 regulates eosinophils, which produce NGF to promote axonal outgrowth. Data are presented as mean ± SEM. P values were calculated by Kruskal-Wallis test with Dunn's multiple comparisons test (*A*), two-way ANOVA and Tukey's post hoc test (*F*–*H*), and two-tailed unpaired Welch's t test (*I*). ns $P > 0.05$, $*P \leq 0.05$, $**P \leq 0.01$, $***P \leq 0.001$, $****P \leq 0.0001$ (scale bars: *C*, 40 μm; *D*, 30 μm).

revealed that the sympathetic activation led to the cellular release of IL-33 by the stromal cell via the adrenergic signal, which then acted on ILC2s and induced IL-5 production. IL-5 was crucial for regulating the adipose eosinophils, which subsequently modulated intra-adipose axonal outgrowth. The data together have discovered a previously unknown mechanism of nerve-immune crosstalk in modifying neuronal control of the WAT, and an overview for graphic summary is shown in Fig. 7*J*.

The sympathetic neurites are established in iWAT during development (47); however, the precise cellular mechanism for the developmental innervation remains unclear. NGF functions as a critical neurotrophic factor for the sympathetic arborizations across multiple tissues and organs (30, 48). Our results showed that sympathetic innervations did not change significantly under steady states upon hematopoietic deletion of *Ngf*, suggesting that the immune cell–derived NGF plays important roles in acute stimuli but is dispensable for establishing innervation during development. Interestingly, the expression of NGF was found in cell types including an adipocyte cell line (3T3L1), mesenchymal stem cells from the human fat (49, 50), and murine endothelial cells and stromal cells in our study. It remains to be determined whether NGF derived from nonimmune cells may contribute to the sympathetic innervation during development. On the other hand, the expression of NGF is

detected in the eosinophils from human subjects (51, 52), and NGF derived from eosinophils promotes neurite extension of the PC-12 pheochromocytoma cell line (51), indicating a conserved regulatory role of eosinophils on axonal plasticity during metabolic/immune challenges. Besides, brain-derived neurotrophic factor was shown to influence sympathetic innervation via multiple functions either in the brain (14) or in adipose tissues through expression in a myeloid subset of cold-induced neuroimmune cells (53). The distinct cellular mechanisms underlying the developmental establishment versus the dynamic adaptation of the sympathetic innervations warrant further investigation, which will provide key insights into how the neuronal control of the adipose tissues is established and how it may respond to distinct physiological and pathological challenges.

In the adipose tissues, eosinophils play important functions in regulating metabolic activity (27, 54–56). Other immune cell types such as ILC2s (22–24), regulatory T cells (34, 57), macrophages (26), and stromal cells (40, 41, 58) are among the critical components in the WAT homeostasis which could influence the number or activation states of eosinophils. For instance, macrophages could affect adipocyte browning independent of nerve innervation (59). Macrophage subsets (60, 61) such as sympathetic nerve–associated macrophages (62) and IL-33–expressing cells (41) are closely associated with the sympathetic nerves, hinting at a complex and interactive network across the nerves and immune cells. Moreover, T cells in the WAT also produced IL-5 and may play a significant role in regulating nerve plasticity, particularly in inflammatory settings such as in obesity or aging. Additionally, the function of eosinophils in regulating airway nerve density is observed in asthmatic conditions (63), suggesting a potential role in modulating neuronal activity in other organs and pathological conditions. It remains to be studied how eosinophils may interplay with a wide array of immune cells in the tissue microenvironment, which consequently affects the neuronal output.

The direct signaling of NE from sympathetic adrenergic nerves to WAT may occur in various cell types. We found here that the stromal cells expressed *Adrα1b*, responded to the stimulation by NE, and initiated calcium flux. The immune cells highly express β2 adrenergic receptor (*Adrβ2*), which confers their responsiveness to NE. However, no significant effect on adipose metabolism was observed upon deletion of *Adrβ2* in macrophage or ILC2s (64, 65). It is yet to be known how adrenergic signaling may affect the cellular pathways in the adipose immune cells and thereby influence energy homeostasis.

The emerging interests in intercellular interactions, such as across the nervous and the immune systems, have advanced our understanding of integrative tissue physiology. We adopted the WAT as an experimental model and showed that the immune subset of eosinophils could influence the sympathetic innervation through regulating axonal outgrowth and nerve density. In-depth studies on the crosstalk in many of the innervated organs will yield further insights into the nerve-immune communications in achieving tissue and systemic homeostasis and in regulating metabolic disease conditions.

Methods

Materials and Correspondence. Further information and requests for resources and reagents should be directed to and will be fulfilled by the corresponding author, Wenwen Zeng (email: wenwenzeng@tsinghua.edu.cn).

Animal Information. All the experimental procedures in mice were performed in compliance with the protocol approved by the Institutional Animal Care and Use Committee of Tsinghua University.

Animals were maintained on the 12-h light/12-h dark cycles with the chow diet and water available ad libitum. Mice utilized in the experiments were at the age of 4 to 12 wk. WT C57BL/6 mice were purchased from Charles River International. Vav^{iCre} (JAX 008610, RRID: IMSR_JAX:008610), $Th^{CreERT2}$ (JAX 025614, RRID: IMSR_JAX:025614), *hM3Dq* (JAX 026220, RRID: IMSR_JAX:026220), *Ai32* (JAX 012569, RRID: IMSR_JAX:012569), and "Red5" IL-5-tdTomato reporter (JAX 030926, RRID: IMSR_JAX:030926) were from the Jackson Laboratory.

$Ngf^{fl/fl}$ mice were generated with targeting vector containing the loxP sites inserted to flank exon 4 of the *Ngf* gene. The linearized targeting donor DNA fragment was delivered together with Cas9 mRNA and single guide RNA (sgRNA) (5′-sgRNA1: 5′-GTGGATTGGCCTCCTTACACAGG-3′; 3′-sgRNA2: 5′-GCTCAGGTAGCAACTATCGGTGG-3′) into C57BL/6 mouse zygotes via microinjection. The resulting offspring were screened by PCR genotyping, DNA sequencing, and Southern blot to select the targeted mice. The mice were bred in house to produce the littermates, which were randomly assigned to experimental groups.

$Epx^{iCreERT2}$ mice were generated by insertion of *P2A-iCreERT2* cassette before the stop codon of *Epx* gene. The targeting vector was constructed with *P2A* site followed by the *iCreERT2* sequence immediately before the stop codon of the *Epx* coding region. Linearized targeting vector was delivered together with Cas9 mRNA and sgRNA (5′-GAACCCTCATTTGCCTCGCC-3′) into C57BL/6 mouse zygotes via microinjection. The resulting offspring were screened by PCR genotyping, DNA sequencing, and Southern blot to select the targeted mice. The mice were crossed to *Ai32* reporter mice for the flow cytometric analysis of cell-specific recombination. To induce genetic recombination in eosinophils, tamoxifen (MACKLIN) in corn oil (100 mg/kg) was intraperitoneally injected to mice of indicated genotype daily for 5 d, and the mice were then analyzed 11 d posttreatment.

$Il33^{-/-}$ mouse line was generated by disruption between exon 1 and exon 4. Cas9 mRNA and sgRNA (5′-sgRNA1: 5′-CAGCACCGCAGGCGAAGCCCTGG-3′; 3′-sgRNA2: 5′-TACTGCATGAGACTCCGTTCTGG-3′) were delivered into C57BL/6 mouse zygotes via microinjection. The resulting offspring were screened by PCR genotyping, DNA sequencing, RT-PCR, and immunostaining to select the targeted mice.

$Il1rl1^{-/-}$ mouse line was generated by disruption between exon 1 and exon 3. Cas9 mRNA and sgRNA (5′-GTGGTCACCAAACCATACCCAGG-3′) were delivered into C57BL/6 mouse zygotes via microinjection. The resulting offspring were screened by PCR genotyping, DNA sequencing, and RT-PCR to select the targeted mice.

For the treatment of the mice to cold exposure, the mice of indicated genotypes were housed at thermoneutral condition (32 °C) for two weeks and transferred to 4 °C for 2 to 6 d, and a longer treatment period was used to determine the nerve density change and beiging and shorter period for analyzing eosinophil. For the experiments of IL-5 neutralization, the anti–IL-5 neutralizing antibody was administrated to the WT mice at 15 mg/kg body weight via intraperitoneal injection twice. The first injection was performed at 3 d before the cold treatment and the second at 1 d of cold treatment. For the experiments of IL-33 treatment, the WT mice were housed at the TN condition. Vehicle (phosphate-buffered saline, PBS) or recombinant murine IL-33 (30 μg/kg, expressed and purified from *Escherichia coli*) was injected intraperitoneally daily for 3 to 6 d.

For the treatment of the mice by CNO, the mice were housed at room temperature. Vehicle (saline) or CNO (1 mg/kg) was injected intraperitoneally for 6 h before iWAT and blood were collected for qPCR and ELISA analysis.

Human Adipose Tissues. The human adipose tissues were collected at the Department of Obstetrics and Gynecology, Ren Ji Hospital. The study was conducted in compliance with the ethical guidelines of the US Common Rule, and the protocol was approved by the Institutional Ethics Committee of Ren Ji Hospital. Written informed consent was signed by all the patients. The normal adipose tissues were collected from 18 patients (females of 27 to 55 y old) during the surgical resection of ovarian cyst or debulking surgery of ovarian carcinomas, followed by the whole-mount immunostaining procedure. The imaging results showed consistency across patients, and representative images are shown.

Antibodies for Immunostaining. Primary antibodies used for immunostaining were rabbit anti-TH (Millipore catalog no. AB152, RRID: AB_390204), rabbit anti-STMN2 (Novus Biologicals catalog no. NBP1-49461, RRID: AB_10011568), mouse anti-Tuj1 (BioLegend catalog no. 801202, RRID: AB_10063408), rabbit anti-Tuj1 (Cell Signaling Technology catalog no. 5568, RRID: AB_10694505), rabbit anti-PGP9.5/UCHL1 (Proteintech catalog no. 14730–1-AP, RRID: AB_2210497), goat anti-VAChT (Millipore catalog no. ABN100, RRID: AB_2630394), rabbit anti-UCP1 (Abcam catalog no. ab10983, RRID: AB_2241462), goat anti-mouse IL-33 (R&D Systems catalog no. AF3626, RRID: AB_884269), goat anti-human IL-33 (R&D Systems catalog no. AF3625, RRID: AB_1151900), mouse anti-human Siglec-8 (BioLegend catalog no. 347102, RRID: AB_2239311), rat anti-Siglec-F-PE (BD Biosciences catalog no. 552126, RRID: AB_394341), rat anti-mouse CD45-PE

(BioLegend catalog no. 103106, RRID: AB_312971), rat anti-human CD45-FITC (BioLegend catalog no. 368508, RRID: AB_2566368), rat anti-CD31 (BD Biosciences catalog no. 553370, RRID: AB_394816). In addition, Alexa Fluor dye–conjugated secondary antibodies were from Thermo Fisher Scientific. Anti–IL-5 neutralizing antibody was from BioXCell (Bio X Cell, catalog no. BE0198, RRID: AB_10950522), and the IgG isotype control was from BioXCell (Bio X Cell, catalog no. BE0083, RRID: AB_1107784).

Whole-Mount Immunostaining and Volume Fluorescence Imaging. The volume fluorescence imaging procedure of WAT was performed as reported (7). In brief, the mice of indicated conditions were anesthetized and perfused with PBS containing 10 μg/mL heparin (Sigma-Aldrich). WAT were dissected out and fixed in PBS/1% paraformaldehyde (PFA)/10% sucrose. The human adipose tissues were also fixed in PBS/1% PFA/10% sucrose. The tissues were washed with PBS and dehydrated with increasing concentration of methanol. The tissues were then bleached with 5% H_2O_2 (1 volume of 30% H_2O_2 diluted in 5 volumes of 100% methanol) containing 10 mM ethylenediaminetetraacetic acid (EDTA) (pH 8.0) and rehydrated with decreasing concentrations of methanol. The tissues were permeabilized in PBS/0.2% TritonX-100/20% dimethyl sulfoxide (DMSO)/ 0.3 M glycine and blocked in PBS/0.2% TritonX-100/10% DMSO/5% donkey serum (Jackson ImmunoResearch). For the staining of Siglec-F, the fixed tissues were permeabilized without dehydration/bleaching/rehydration steps. The tissues were then incubated with indicated primary antibodies diluted (1:500 to 1:1,000) in PBS/0.2% Tween-20/10 μg/mL heparin/5% DMSO/5% donkey serum and washed in PBS/0.2% Tween-20/10 μg/mL heparin. The tissues were incubated with indicated Alexa dye–conjugated secondary antibodies diluted (1:500) in PBS/0.2% Tween-20/10 μg/mL heparin/5% donkey serum and washed in PBS/0.2% Tween-20/10 μg/mL heparin before the tissue clearing. Immunolabeled WAT were embedded in 1% agarose blocks prepared in PBS, followed by dehydration, optical clearing, and volume imaging by lightsheet microscopy (7). The image stacks were acquired by the continuous lightsheet scanning method without the contrast-blending algorithm.

Imaris was used to reconstruct the image stacks obtained from the lightsheet imaging. Then, 3D projections of the image stacks were generated with the orthogonal perspective for the representative images shown in figures. Image stacks of WAT from cold-challenged WT mice were used to reconstruct the movie. For the display purpose, nonspecific signals were removed by the Surface function. Movies of the image stacks were generated with a frame rate of 15 fps. Masked signals generated by the Surface function were used for the representative images of mouse IL-33 staining.

For the quantification of eosinophils, four cubic regions from each iWAT were randomly selected and masked by the Surface function of Imaris. The siglec-F signals were constructed by the Spots function of Imaris. The density of eosinophils was calculated as spots count/surface volume (number per cube millimeter).

For the quantification of nerve fibers, 5 to 10 cubic regions from each iWAT were randomly selected and masked by the Surface function of Imaris. The TH or STMN2 signals in each cubic region were automatically traced by the Filament function of Imaris. The density of nerve fibers was calculated as filament length/surface volume (mm/mm^3).

For the quantification of vasculature, 5 to 10 cubic regions from each iWAT were randomly selected and masked by the Surface function of Imaris. The vasculature in each cubic region was automatically traced by the Filament function of Imaris. The $CD31^+$ vascular density was calculated as filament length/surface volume (mm/mm^3).

For quantification of the distances from CD45, siglec-F or IL-33 signals to nerve fibers, their signals were constructed by the Spots function of Imaris. The TH signals were constructed by the Surface function of Imaris. The shortest distances from spots to surface were measured and used for the curve.

ELISA Analysis. The mice were killed by cervical dislocation. The iWAT were homogenized in the extraction buffer [100 mM Tris·HCl (pH 7.4), 150 mM NaCl, 1 mM ethylene glycol tetraacetic acid (EGTA), 1 mM EDTA, 1% Triton X-100, 0.5% sodium deoxycholate, protease inhibitor mixture, and 1 mM phenylmethylsulfonyl fluoride (PMSF)] after the removal of the inguinal lymph node. The samples were then centrifuged for 20 min at 13,000 rpm at 4 °C to remove cell debris and lipid. The samples were then measured and quantified by the β-NGF ELISA kit (R&D, DY556) with two- or fivefold dilutions. All standards and samples were assayed in duplicate. The concentrations were calculated according to the instructions from the manufacturer.

For IL-5 ELISA of ILC2s, WT mice were injected with recombinant IL-33 intraperitoneally for 6 d. ILC2s were sort purified ($CD45^+Lin^-CD90.2^+Sca1^{hi}KLRG1^+$) from adipose tissues and cultured in Roswell Park Memorial Institute (RPMI) culture media with 10% (vol/vol) heat-inactivated fetal bovine serum (FBS), 100 U/mL penicillin/streptomycin, 10 mM Hepes buffer, nonessential amino acids, 1 mM sodium pyruvate, and 50 μM 2-mercaptoethanol. Lineage-negative gating (Lin^-) includes markers for CD3, CD4, CD5, CD8, B220, CD11c, CD11b, Gr-1, TER119, and NK1.1. The cells were expanded for three days with the addition of 10 ng/mL IL-2 (51061-MNAE-20; Sino Biological) and 10 ng/mL IL-7 (50217-MNAE-20; Sino Biological) before further stimulation. ILC2s were washed and rested for 4 h at 37 °C and then stimulated with 10 ng/mL IL-7 or 10 ng/mL IL-7 and 10 ng/mL IL-33 for 6 h. Cell culture media were collected for the IL-5 ELISA analysis (431204; BioLegend) at 1:100 dilution.

For IL-5 ELISA of mouse serum, whole blood was collected in untreated tube and incubated at room temperature for 20 min. After centrifugation at 1,000 to 2,000 × *g* for 10 min in a refrigerated centrifuge, the supernatant was collected and measured by the IL-5 ELISA kit (catalog no. 431204; BioLegend) with twofold dilution. All standards and samples were assayed in duplicate. The sensitivity of the kit is 4 pg/mL, and the standard range is 7.8 to 500 pg/mL.

In Vitro Cultures. For the cocultures of SCG and eosinophils, the ganglia were dissected from P1 neonatal WT mice. After washing once with Dulbecco's modified Eagle's medium (DMEM) (Corning), the ganglia were seeded in the center of poly-D-lysine (Sigma-Aldrich)–coated 24-well plates. Eosinophils were sort purified ($Siglec\text{-}F^+CCR3^+$) from the peritoneal cavity of WT mice intraperitoneally injected with recombinant IL-33 for 3 d. Then, 300,000 eosinophils in 200 μL complete RPMI-1640 media with 10% (vol/vol) heat-inactivated FBS and 100 U/mL penicillin/streptomycin were mixed with 200 μL neurobasal/B27 media (Thermo Fisher Scientific) supplemented with 0.25% methyl-cellulose and then added to the wells. The anti-NGF neutralization antibody was added at a concentration of 50 μg/mL 36 h after coculture, and SCG were fixed in PBS/1% PFA, immunostained with anti-TH followed by corresponding Alexa dye–conjugated secondary antibody, and imaged by fluorescence microscope. Images were then analyzed using the NeuriteJ plug-in for ImageJ, as previously reported (29). The number of intersections was plotted against the distance from the ganglia body, and the AUC was extrapolated as an indicator of axonal growth.

For the culture of eosinophils, WT mice were injected with recombinant IL-33 intraperitoneally for 3 to 6 d. Eosinophils from the peritoneal cavity were then sort purified ($Siglec\text{-}F^+CCR3^+$) and cultured in complete RPMI-1640 media with 10% (vol/vol) heat-inactivated FBS and 100 U/mL penicillin/streptomycin and 10 ng/mL IL-5. For the detection of released NGF, 3.5×10^5 cells were seeded to each well of a 96-well ELISA plate precoated with the capture antibody. The cells were then stimulated with 0.1 mg/mL C48/80 for 3 h at 37 °C, after which the cells were washed away and the plate was processed for the detection of released NGF protein.

Calcium Imaging. Stromal cells (sort purified as $7AAD^-TER119^-CD45^-$) from WAT were cultured in complete DMEM media with 10% (vol/vol) heat-inactivated FBS and 100 U/mL penicillin/streptomycin. The cells were washed once with Hanks' balanced salt solution (HBSS) buffer (1×HBSS with 1.26 mM Ca^{2+} and 10 mM Hepes) before being loaded with 2 μM calcium indicator Rhod-2 acetoxymethyl ester (R1245MP; Thermo Fisher Scientific) for 30 min at 37 °C. Then, cells were washed twice and maintained in 200 μL HBSS buffer for live cell imaging. After basal Ca^{2+} concentration was monitored, the cells were added with 5 μg/mL ionomycin and 1 mM NE or PE followed by immediate imaging. Rhod-2 fluorescence was measured using PerkinElmer Opera phenix. The images and movies were generated using HARMONY software. For the kinetics data, the Rhod-2 fluorescence intensity was normalized to the basal intensity.

Statistical Analysis. The data were analyzed with GraphPad Prism. For the comparisons of two groups, *P* values were calculated by unpaired two-tailed Student's *t* test. Welch's correction was used when the variances of the samples were unequal. For the comparisons of gene expression among three or more groups, one-way ANOVA was used. For the comparisons of four groups, two-way ANOVA (genotype and treatment) and Tukey's multiple comparisons test were applied on samples.

Data Availability. All study data are included in the article and/or supporting information.

ACKNOWLEDGMENTS. This work was supported by the National Key R&D Program of China (2017YFA0505800) and the National Natural Science Foundation of China (31822018, 31770936, 91742106, 81802585, and 81922047). The work was also supported by the Center for Life Sciences and the Institute for Immunology at Tsinghua University.

1. A. Caron, S. Lee, J. K. Elmquist, L. Gautron, Leptin and brain-adipose crosstalks. *Nat. Rev. Neurosci.* **19**, 153–165 (2018).
2. A. Guilherme, F. Henriques, A. H. Bedard, M. P. Czech, Molecular pathways linking adipose innervation to insulin action in obesity and diabetes mellitus. *Nat. Rev. Endocrinol.* **15**, 207–225 (2019).
3. T. J. Bartness, M. Bamshad, Innervation of mammalian white adipose tissue: Implications for the regulation of total body fat. *Am. J. Physiol.* **275**, R1399–R1411 (1998).
4. B. Cannon, J. Nedergaard, Brown adipose tissue: Function and physiological significance. *Physiol. Rev.* **84**, 277–359 (2004).
5. P. E. Scherer, The many secret lives of adipocytes: Implications for diabetes. *Diabetologia* **62**, 223–232 (2019).
6. J. M. Friedman, C. S. Mantzoros, 20 years of leptin: From the discovery of the leptin gene to leptin in our therapeutic armamentarium. *Metabolism* **64**, 1–4 (2015).
7. H. Jiang, X. Ding, Y. Cao, H. Wang, W. Zeng, Dense intra-adipose sympathetic arborizations are essential for cold-induced beiging of mouse white adipose tissue. *Cell Metab.* **26**, 686–692.e3 (2017).
8. J. Chi *et al.*, Three-dimensional adipose tissue imaging reveals regional variation in beige fat biogenesis and PRDM16-dependent sympathetic neurite density. *Cell Metab.* **27**, 226–236.e3 (2018).
9. A. Caron *et al.*, POMC neurons expressing leptin receptors coordinate metabolic responses to fasting via suppression of leptin levels. *eLife* **7**, e33710 (2018).
10. W. Zeng *et al.*, Sympathetic neuro-adipose connections mediate leptin-driven lipolysis. *Cell* **163**, 84–94 (2015).
11. I. Murano, G. Barbatelli, A. Giordano, S. Cinti, Noradrenergic parenchymal nerve fiber branching after cold acclimatisation correlates with brown adipocyte density in mouse adipose organ. *J. Anat.* **214**, 171–178 (2009).
12. A. Giordano *et al.*, Regional-dependent increase of sympathetic innervation in rat white adipose tissue during prolonged fasting. *J. Histochem. Cytochem.* **53**, 679–687 (2005).
13. A. Vitali *et al.*, The adipose organ of obesity-prone C57BL/6J mice is composed of mixed white and brown adipocytes. *J. Lipid Res.* **53**, 619–629 (2012).
14. P. Wang *et al.*, A leptin-BDNF pathway regulating sympathetic innervation of adipose tissue. *Nature* **583**, 839–844 (2020).
15. Y. Cao, H. Wang, W. Zeng, Whole-tissue 3D imaging reveals intra-adipose sympathetic plasticity regulated by NGF-TrkA signal in cold-induced beiging. *Protein Cell* **9**, 527–539 (2018).
16. A. Guilherme *et al.*, Adipocyte lipid synthesis coupled to neuronal control of thermogenic programming. *Mol. Metab.* **6**, 781–796 (2017).
17. A. Guilherme *et al.*, Neuronal modulation of brown adipose activity through perturbation of white adipocyte lipogenesis. *Mol. Metab.* **16**, 116–125 (2018).
18. X. Zeng *et al.*, Innervation of thermogenic adipose tissue via a calsyntenin 3β-S100b axis. *Nature* **569**, 229–235 (2019).
19. Y. Wolf *et al.*, Brown-adipose-tissue macrophages control tissue innervation and homeostatic energy expenditure. *Nat. Immunol.* **18**, 665–674 (2017).
20. B. Hu *et al.*, γδ T cells and adipocyte IL-17RC control fat innervation and thermogenesis. *Nature* **578**, 610–614 (2020).
21. M. Blaszkiewicz *et al.*, Neuropathy and neural plasticity in the subcutaneous white adipose depot. *PLoS One* **14**, e0221766 (2019).
22. A. B. Molofsky *et al.*, Innate lymphoid type 2 cells sustain visceral adipose tissue eosinophils and alternatively activated macrophages. *J. Exp. Med.* **210**, 535–549 (2013).
23. M. W. Lee *et al.*, Activated type 2 innate lymphoid cells regulate beige fat biogenesis. *Cell* **160**, 74–87 (2015).
24. J. R. Brestoff *et al.*, Group 2 innate lymphoid cells promote beiging of white adipose tissue and limit obesity. *Nature* **519**, 242–246 (2015).
25. F. Villarroya, R. Cereijo, J. Villarroya, A. Gavaldà-Navarro, M. Giralt, Toward an understanding of how immune cells control brown and beige adipobiology. *Cell Metab.* **27**, 954–961 (2018).
26. S. M. Reilly, A. R. Saltiel, Adapting to obesity with adipose tissue inflammation. *Nat. Rev. Endocrinol.* **13**, 633–643 (2017).
27. D. Wu *et al.*, Eosinophils sustain adipose alternatively activated macrophages associated with glucose homeostasis. *Science* **332**, 243–247 (2011).
28. R. R. Rao *et al.*, Meteorin-like is a hormone that regulates immune-adipose interactions to increase beige fat thermogenesis. *Cell* **157**, 1279–1291 (2014).
29. A. Torres-Espín, D. Santos, F. González-Pérez, J. del Valle, X. Navarro, Neurite-J: An image-J plug-in for axonal growth analysis in organotypic cultures. *J. Neurosci. Methods* **236**, 26–39 (2014).
30. N. O. Glebova, D. D. Ginty, Heterogeneous requirement of NGF for sympathetic target innervation in vivo. *J. Neurosci.* **24**, 743–751 (2004).
31. J. Wu *et al.*, Beige adipocytes are a distinct type of thermogenic fat cell in mouse and human. *Cell* **150**, 366–376 (2012).
32. C. Joseph *et al.*, Deciphering hematopoietic stem cells in their niches: A critical appraisal of genetic models, lineage tracing, and imaging strategies. *Cell Stem Cell* **13**, 520–533 (2013).
33. L. Aloe, M. L. Rocco, P. Bianchi, L. Manni, Nerve growth factor: From the early discoveries to the potential clinical use. *J. Transl. Med.* **10**, 239 (2012).
34. A. Vasanthakumar *et al.*, The transcriptional regulators IRF4, BATF and IL-33 orchestrate development and maintenance of adipose tissue-resident regulatory T cells. *Nat. Immunol.* **16**, 276–285 (2015).
35. D. Kolodin *et al.*, Antigen- and cytokine-driven accumulation of regulatory T cells in visceral adipose tissue of lean mice. *Cell Metab.* **21**, 543–557 (2015).
36. T. Y. F. Halim *et al.*, Tissue-restricted adaptive type 2 immunity is orchestrated by expression of the costimulatory molecule OX40L on group 2 innate lymphoid cells. *Immunity* **48**, 1195–1207 (2018).
37. A. M. Miller *et al.*, Interleukin-33 induces protective effects in adipose tissue inflammation during obesity in mice. *Circ. Res.* **107**, 650–658 (2010).
38. J. M. Han *et al.*, IL-33 reverses an obesity-induced deficit in visceral adipose tissue ST2+ T regulatory cells and ameliorates adipose tissue inflammation and insulin resistance. *J. Immunol.* **194**, 4777–4783 (2015).
39. M. Hashiguchi *et al.*, IL-33 activates eosinophils of visceral adipose tissue both directly and via innate lymphoid cells. *Eur. J. Immunol.* **45**, 876–885 (2015).
40. T. Mahlakõiv *et al.*, Stromal cells maintain immune cell homeostasis in adipose tissue via production of interleukin-33. *Sci. Immunol.* **4**, eaax0416 (2019).
41. R. G. Spallanzani *et al.*, Distinct immunocyte-promoting and adipocyte-generating stromal components coordinate adipose tissue immune and metabolic tenors. *Sci. Immunol.* **4**, eaaw3658 (2019).
42. J. C. Nussbaum *et al.*, Type 2 innate lymphoid cells control eosinophil homeostasis. *Nature* **502**, 245–248 (2013).
43. P. C. Schwalie *et al.*, A stromal cell population that inhibits adipogenesis in mammalian fat depots. *Nature* **559**, 103–108 (2018).
44. J. Akinaga, J. A. García-Sáinz, A. S Pupo, Updates in the function and regulation of α_1-adrenoceptors. *Br. J. Pharmacol.* **176**, 2343–2357 (2019).
45. H. Kouzaki, K. Iijima, T. Kobayashi, S. M. O'Grady, H. Kita, The danger signal, extracellular ATP, is a sensor for an airborne allergen and triggers IL-33 release and innate Th2-type responses. *J. Immunol.* **186**, 4375–4387 (2011).
46. B. L. Roth, DREADDs for neuroscientists. *Neuron* **89**, 683–694 (2016).
47. J. Chi *et al.*, Early postnatal interactions between beige adipocytes and sympathetic neurites regulate innervation of subcutaneous fat. *eLife* **10**, e64693 (2021).
48. C. Crowley *et al.*, Mice lacking nerve growth factor display perinatal loss of sensory and sympathetic neurons yet develop basal forebrain cholinergic neurons. *Cell* **76**, 1001–1011 (1994).
49. S. T. Hsiao *et al.*, Comparative analysis of paracrine factor expression in human adult mesenchymal stem cells derived from bone marrow, adipose, and dermal tissue. *Stem Cells Dev.* **21**, 2189–2203 (2012).
50. M. R. Peeraully, J. R. Jenkins, P. Trayhurn, NGF gene expression and secretion in white adipose tissue: Regulation in 3T3-L1 adipocytes by hormones and inflammatory cytokines. *Am. J. Physiol. Endocrinol. Metab.* **287**, E331–E339 (2004).
51. H. Kobayashi, G. J. Gleich, J. H. Butterfield, H. Kita, Human eosinophils produce neurotrophins and secrete nerve growth factor on immunologic stimuli. *Blood* **99**, 2214–2220 (2002).
52. A. Solomon *et al.*, Nerve growth factor is preformed in and activates human peripheral blood eosinophils. *J. Allergy Clin. Immunol.* **102**, 454–460 (1998).
53. M. Blaszkiewicz *et al.*, The involvement of neuroimmune cells in adipose innervation. *Mol. Med.* **26**, 126 (2020).
54. Y. Qiu *et al.*, Eosinophils and type 2 cytokine signaling in macrophages orchestrate development of functional beige fat. *Cell* **157**, 1292–1308 (2014).
55. P. F. Weller, L. A. Spencer, Functions of tissue-resident eosinophils. *Nat. Rev. Immunol.* **17**, 746–760 (2017).
56. D. Brigger *et al.*, Eosinophils regulate adipose tissue inflammation and sustain physical and immunological fitness in old age. *Nat. Metab.* **2**, 688–702 (2020).
57. M. Feuerer *et al.*, Lean, but not obese, fat is enriched for a unique population of regulatory T cells that affect metabolic parameters. *Nat. Med.* **15**, 930–939 (2009).
58. B. M. J. Rana *et al.*, A stromal cell niche sustains ILC2-mediated type-2 conditioning in adipose tissue. *J. Exp. Med.* **216**, 1999–2009 (2019).
59. F. Henriques *et al.*, Single-cell RNA profiling reveals adipocyte to macrophage signaling sufficient to enhance thermogenesis. *Cell Rep.* **32**, 107998 (2020).
60. C. D. Camell *et al.*, Inflammasome-driven catecholamine catabolism in macrophages blunts lipolysis during ageing. *Nature* **550**, 119–123 (2017).
61. I. Ruiz de Azua *et al.*, Adipocyte cannabinoid receptor CB1 regulates energy homeostasis and alternatively activated macrophages. *J. Clin. Invest.* **127**, 4148–4162 (2017).
62. R. M. Pirzgalska *et al.*, Sympathetic neuron-associated macrophages contribute to obesity by importing and metabolizing norepinephrine. *Nat. Med.* **23**, 1309–1318 (2017).
63. M. G. Drake *et al.*, Eosinophils increase airway sensory nerve density in mice and in human asthma. *Sci. Transl. Med.* **10**, eaar8477 (2018).
64. K. Petkevicius *et al.*, Macrophage beta2-adrenergic receptor is dispensable for the adipose tissue inflammation and function. *Mol. Metab.* **48**, 101220 (2021).
65. F. Cardoso *et al.*, Neuro-mesenchymal units control ILC2 and obesity via a brain-adipose circuit. *Nature* **597**, 410–414 (2021).